

# Exploring the Feasible Regulation Region of Building HVAC Systems Within Hygro-Thermal Comfort

Taoyi Qi<sup>ID</sup>, *Graduate Student Member, IEEE*, Hongxun Hui<sup>ID</sup>, *Senior Member, IEEE*, and Yonghua Song<sup>ID</sup>, *Fellow, IEEE*

**Abstract**—Heating, Ventilation, and Air Conditioning (HVAC) systems are widely recognized as promising demand response (DR) resources for enhancing grid flexibility. Despite extensive research on evaluating the regulation capacity of HVAC systems, the role of humidity in air dynamic description and occupant comfort assessment during DR has been overlooked. This paper addresses these gaps by exploring the feasible regulation region of HVAC systems while meeting occupant hygro-thermal comfort. Firstly, a comprehensive model of HVAC systems is developed to describe the hygro-thermal air dynamics and equipment characteristics. Subsequently, the hygro-thermal comfort area is defined to establish permissible temperature and humidity boundaries. Based on key constraints, the hygro-thermal air dynamics are categorized into 3 distinct types. Moreover, a novel criterion is proposed to identify these dynamics without requiring full knowledge of boundary conditions. On this basis, the maximum regulation capacities are quantitatively evaluated to explore the feasible regulation region throughout the day. Finally, numerical case studies are conducted to validate the proposed approach. The results demonstrate that humidity plays a crucial role in the operating power and the feasible regulation region of HVAC systems. Incorporating humidity improves hygro-thermal comfort, thereby encouraging more occupant participation in DR programs.

**Index Terms**—Power systems, demand response, HVAC systems, capacity evaluation, hygro-thermal comfort.

## I. INTRODUCTION

POWER systems are transitioning from fossil fuel power plants to renewable energy sources (RESs) to promote a sustainable future and achieve carbon neutrality [1].

Received 25 November 2024; revised 9 March 2025 and 28 April 2025; accepted 3 May 2025. Date of publication 16 May 2025; date of current version 23 June 2025. This work was supported in part by the Electric Power Research Institute of Guizhou Power Grid Company Ltd. under Project GZKJXM20240010; in part by the National Natural Science Foundation of China under Grant 524B2100 and Grant 52407075; in part by the State Key Laboratory of Power System Operation and Control under Grant SKLD24KM11; and in part by the Science and Technology Development Fund, Macau, SAR, under Grant 001/2024/SKL. Paper no. TSG-02041-2024. (Corresponding author: Hongxun Hui.)

The authors are with the State Key Laboratory of Internet of Things for Smart City, University of Macau, Macau, China, and also with the Laboratory of Internet of Things for Smart City, Advanced Research Institute in Hengqin, University of Macau, Zhuhai 519031, China (e-mail: taoyi.qi@conncet.um.edu.mo; hongxunhui@um.edu.mo; yhsong@um.edu.mo).

Color versions of one or more figures in this article are available at <https://doi.org/10.1109/TSG.2025.3569074>.

Digital Object Identifier 10.1109/TSG.2025.3569074

The inherent output uncertainty and intermittency of RESs necessitate additional regulation capacities to maintain the supply-demand balance [2]. Furthermore, the decommissioning of power plants exacerbates the insufficiency of regulation capacities [3], particularly in cities with higher load densities [4]. In response to these challenges, demand response (DR) programs have emerged to harness regulation capacities from various flexible resources at the demand side [5], [6].

Buildings, accounting for nearly 40% of global energy consumption [7], contain numerous flexible resources and play a critical role in DR. Among these, Heating, Ventilation, and Air Conditioning (HVAC) systems are widely recognized as promising DR resources, owing to their substantial energy proportions within buildings [8]. Benefiting from the inherent hygro-thermal inertia, occupant comfort can be maintained during short periods of regulation or interruption [9]. Since Lu [10] innovatively proposed using HVAC systems for load-balancing services in power systems in 2012, studies on HVAC utilization have advanced significantly. Focusing on massive aggregated residential air conditioners, Büning et al. [11] proposed a robust model predictive approach for providing operating reserves. Furthermore, a data-driven method was introduced in [12] to evaluate the DR potential of residential air conditioners equipped with smart meters. Other services, such as frequency regulation [13], RESs accommodation [14], and voltage regulation [15], have also been explored to meet the multi-time scale regulation needs of power systems.

Ensuring occupant comfort is the top priority for HVAC systems [16]. Accurate evaluation of regulation capacities is crucial for leveraging most DR potential without noticeable comfort loss [17]. Typically, the maximum regulation capacity is evaluated based on an acceptable temperature interval by establishing the relationship between temperature variations and power adjustments. The equivalent thermal parameter (ETP) model is commonly used to depict temperature dynamics, owing to its great balance between accuracy and simplicity. For instance, the optimal on/off periods for HVAC providing frequency regulation services were calculated using the ETP model [18]. The thermal-electrical model of central air conditioning was established in [19] using the ETP model to facilitate capacity allocation and distributed control. However, factors such as internal heat generation and solar radiation are often ignored in the ETP model to simplify the calculation, which may compromise evaluation accuracy [20], [21].

The absence of humidity leads to more significant deviations than over-simplification. The total cooling load of HVAC systems comprises sensible and latent loads, which are individually related to temperature and humidity (T&H) [22]. Statistical results indicated that the latent load can contribute to half of the total cooling demand, as observed in Pugh Hall at the University of Florida [23]. Ignoring latent load results in inaccurate baseline estimation and corresponding regulation capacities. More seriously, overlooking humidity can adversely affect occupant comfort during DR, especially in humid areas. Therefore, some researchers started to investigate humidity impacts on HVAC system control. Raman et al. [23] introduced a model predictive control method for energy-efficient HVAC operation with comprehensive sensible and latent load consideration. In [24], a hybrid modeling-based approach was proposed for the multi-zone building to precisely describe the coupling relationship between T&H. However, these studies focused on optimal operation under designed conditions rather than DR deployment, limiting their applicability for evaluating the feasible regulation region. Yuan et al. [25] presented a T&H setback strategy to explore the DR potential of HVAC systems by adjusting supply air and chilled water, yet the comprehensive hygro-thermal comfort was not considered.

Hygro-thermal comfort is widely incorporated in HVAC design, as exemplified by ASHRAE Standard 55-2023, which stipulates both T&H boundaries [26]. Kumar et al. [27] presented an adaptive method to define thermal comfort zones for naturally ventilated buildings, accommodating India's cultural and climatic diversity. Schiavon et al. [28] introduced an innovative Web application based on ASHRAE Standard for visualizing thermal comfort. In practice, humidity is not directly controllable in most HVAC systems. Coupled with the complex interplay between T&H, hygro-thermal comfort is seldom considered in DR. However, DR seeks to explore the maximum regulation capacity while maintaining thermal comfort, necessitating the incorporation of humidity into the feasible regulation region by addressing these challenges:

- Tracking the T&H dynamics of zone air, influenced by power regulation, poses a challenge for developing the hygro-thermal model of HVAC systems, particularly due to the close interaction between T&H.
- Incorporating humidity boundaries expands the comfort constraint from a one-dimensional temperature interval to a two-dimensional hygro-thermal area. Identifying the primary factor is essential before exploring the feasible regulation region.

To this end, this paper develops comprehensive models of HVAC systems and defines the hygro-thermal comfort area for occupants. Then, the feasible regulation region of HVAC systems is explored by identifying the primary factor under various conditions. The main contributions are as follows:

1) Comprehensive HVAC system models, including hygro-thermal air dynamics, air conditioning processes, and main equipment features, are developed to describe the relationship between zone air states and power consumption. These models allow for the calculation of coupling T&H dynamics influenced by multiple factors during DR deployment.

2) The hygro-thermal comfort area constrained by T&H is designed to preserve occupant benefits. The varying hygro-thermal dynamics are categorized into 3 types: temperature-dominated, humidity-dominated, and T&H-dominated, to evaluate the regulation capacity at different time instants.

3) A novel criterion is proposed to differentiate the type of hygro-thermal dynamics without full knowledge of boundary conditions, accompanied by a relevant parameter determination method for HVAC systems. Based on the specific dynamic, the feasible regulation region is quantitatively evaluated within hygro-thermal comfort.

## II. MODELING OF BUILDING HVAC SYSTEMS

Water-cooled central air conditioners (CACs) are commonly used in large buildings due to their higher energy efficiency and reduced space requirements. Therefore, CACs are adopted as the HVAC systems for evaluating the feasible regulation region. As shown in Fig. 1, the operation of HVAC systems involves 3 processes, which are modeled to establish relationships between hygro-thermal dynamics and power adjustments.

### A. Model of Hygro-Thermal Dynamics in Cooling Zone

DR programs focus on the aggregate potential of the entire building rather than individual rooms. Hence, the building is treated as a single cooling zone to evaluate its feasible regulation region. The total cooling load for this zone consists of sensible and latent loads.

$$Q_{\text{HVAC}}^t = Q_{\text{HVAC}}^{s,t} + Q_{\text{HVAC}}^{l,t} \quad (1)$$

where  $Q_{\text{HVAC}}^t$  is the total cooling load of the HVAC systems at time  $t$ ;  $Q_{\text{HVAC}}^{s,t}$  and  $Q_{\text{HVAC}}^{l,t}$  represent the sensible and latent cooling loads at time instant  $t$ , respectively. Sensible load relates to temperature changes perceptible to occupants, while latent load corresponds to variations in humidity.

To depict the hygro-thermal comfort during DR events, the first-order ETP model is employed. This model can describe the temperature dynamics influenced by multiple factors [10]:

$$C_z \frac{dT_z^t}{dt} = -Q_{\text{HVAC}}^{s,t} + Q_{\text{env}}^t + Q_{\text{solar}}^t + Q_{\text{occ}}^t \quad (2)$$

$$C_z = \rho_{\text{air}} V_b C_{\text{air}} \quad (3)$$

where  $T_z^t$  is the real-time zone temperature;  $C_z$  mirrors the thermal capacity of the zone;  $Q_{\text{env}}^t$ ,  $Q_{\text{solar}}^t$ , and  $Q_{\text{occ}}^t$  are heat gains from envelop heat conduction, solar radiation, and internal heat sources (e.g., people and equipment), respectively;  $\rho_{\text{air}}$  is the density of air;  $V_b$  is the volume of the building;  $C_{\text{air}}$  is the specific heat of air.

$$Q_{\text{HVAC}}^{s,t} = m_{\text{sa}}^t C_{\text{air}} (T_z^t - T_{\text{sa}}^t) \quad (4)$$

$$Q_{\text{env}}^t = K_{\text{env}} A_{\text{sf}} (T_{\text{oa}}^t - T_z^t) \quad (5)$$

$$Q_{\text{solar}}^t = \gamma_w A_{\text{sf}} \gamma_{\text{SHGC}} R_{\text{solar}}^t \quad (6)$$

$$Q_{\text{occ}}^t = N_{\text{occ}}^t (Q_{\text{occ}} + Q_{\text{equip}}) \quad (7)$$

where  $m_{\text{sa}}^t$  is the mass flow rate of supply air;  $T_{\text{sa}}^t$  and  $T_{\text{oa}}^t$  are the supply air and outdoor air temperatures, respectively;

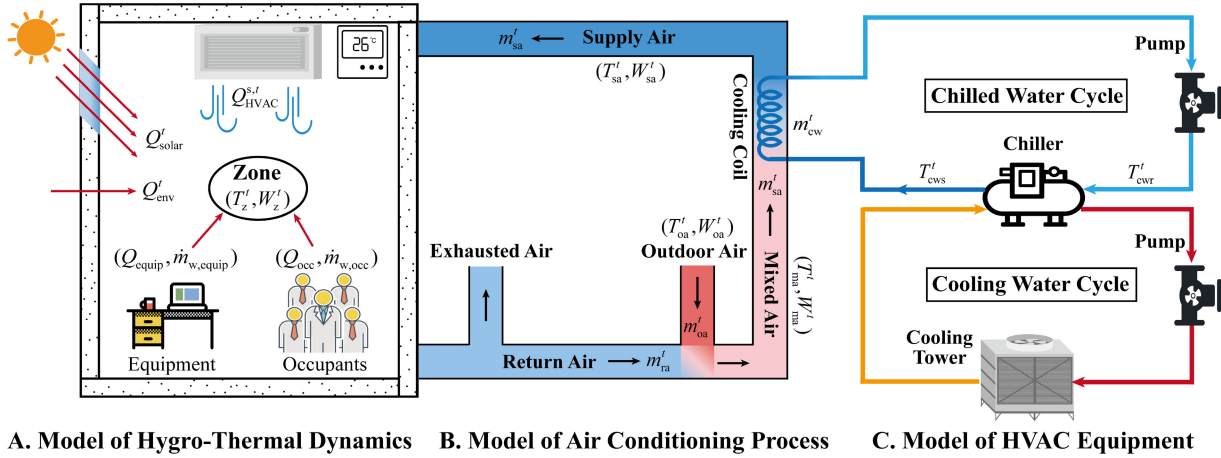


Fig. 1. The developed comprehensive model of HVAC systems considering T&H.

$K_{\text{env}}$  is the heat transfer coefficient of the building envelope;  $A_{\text{sf}}$  is the surface area of the building;  $\gamma_w$  and  $\gamma_{\text{SHGC}}$  represent the windows-wall ratio and the solar heat gain coefficient, respectively;  $R_{\text{solar}}^t$  mirrors the real-time solar radiation;  $Q_{\text{occ}}$  is the heat load per occupant;  $Q_{\text{equip}}$  is the average heat load per occupant from equipment;  $N_{\text{occ}}^t$  is the number of occupants, which can be obtained through direct measurements (e.g., camera-based sensors [29]) or indirect inference (e.g., Wi-Fi data [30]).

The dynamics of zone humidity are influenced by 2 main factors: the dehumidification of the supply air and the water vapor produced by occupants and equipment. The humidity ratio is used to represent the humidity dynamics [31]:

$$\rho_{\text{air}} V_b \frac{dW_z^t}{dt} = m_{\text{sa}}^t (W_{\text{sa}}^t - W_z^t) + N_{\text{occ}}^t (\dot{m}_{w,\text{occ}} + \dot{m}_{w,\text{equip}}) \quad (8)$$

where  $W_z^t$  and  $W_{\text{sa}}^t$  are the humidity ratios of zone air and supply air, respectively;  $\dot{m}_{w,\text{occ}}$  and  $\dot{m}_{w,\text{equip}}$  are the water vapor generated by occupants and equipment, respectively.

The supply air plays a critical role in regulating both T&H. Therefore, accurately determining its state (T&H) is essential for calculating the hygro-thermal dynamics.

### B. Model of Air Conditioning Process

The air conditioning process aims to deliver cool supply air through the air cycle, as shown in Fig. 1. Firstly, a portion of the return air is exhausted, with fresh outdoor air introduced to improve zone air quality. Next, the remaining return air is mixed with the outdoor air. The mass flow rate of supply air is kept constant to maintain air balance.

$$m_{\text{sa}}^t = m_{\text{ra}}^t + m_{\text{oa}}^t \quad (9)$$

where  $m_{\text{ra}}^t$  and  $m_{\text{oa}}^t$  are real-time mass flow rates of the remaining return air and outdoor air, respectively.

Assuming the return air and zone air are in the same state, the mixed air states can be determined based on their specific composition.

$$\begin{cases} T_{\text{ma}}^t = \frac{m_{\text{ra}}^t T_z^t + m_{\text{oa}}^t T_{\text{oa}}^t}{m_{\text{sa}}^t} \\ W_{\text{ma}}^t = \frac{m_{\text{ra}}^t W_z^t + m_{\text{oa}}^t W_{\text{oa}}^t}{m_{\text{sa}}^t} \end{cases} \quad (10)$$

where  $T_{\text{ma}}^t$  and  $W_{\text{ma}}^t$  are the temperature and humidity ratio of the mixed air, respectively;  $T_{\text{oa}}^t$  and  $W_{\text{oa}}^t$  indicate the temperature and humidity ratio of the outdoor air, respectively.

The mixed airflow passes through the cooling coil, where air cooling and dehumidification occur simultaneously. The energy exchange between the mixed air and the cooling coil is represented using enthalpy, which indicates air energy at different states. The enthalpy  $h_a$  of air, with temperature  $T_a$  and humidity ratio  $W_a$ , can be expressed as follows [32]:

$$h_a = 1.005T_a + (1.84T_a + 2500)W_a \quad (11)$$

The enthalpy of supply air can be calculated based on the enthalpy of mixed air and the total cooling capacity provided by HVAC systems:

$$h_{\text{sa}}^t = h_{\text{ma}}^t - Q_{\text{HVAC}}^t / m_{\text{sa}}^t \quad (12)$$

where  $h_{\text{sa}}^t$  and  $h_{\text{ma}}^t$  represent the real-time enthalpy of the supply air and mixed air, respectively.

After obtaining the enthalpy of the supply air, the next obstacle is to determine its specific T&H, as both factors contribute to its enthalpy. Based on engineering experience, the relative humidity (RH) of the supply air is about 90% [33], when the water vapor is saturated during the cooling process. Otherwise, the humidity ratio of supply air is equal to that of mixed air.

The RH of air  $RH_a(W_a, T_a)$  with humidity ratio  $W_a$  and temperature  $T_a$  can be expressed as follows:

$$RH_a(W_a, T_a) = \frac{W_a}{W_{\text{as}}(T_a)} \times 100\% \quad (13)$$

where  $W_{\text{as}}(T_a)$  is the saturated humidity ratio of air at temperature  $T_a$ .

The saturated humidity ratio of air can be calculated based on the maximum partial pressure of water vapor, which is derived from the Antoine equation [34].

$$W_{\text{as}}(T_a) = 622 \frac{p_{\text{ws}}(T_a)}{p_{\text{atm}} - p_{\text{ws}}(T_a)} \quad (14)$$

$$\lg[p_{\text{ws}}(T_a)] = k_a - \frac{k_B}{k_C + T_a} \quad (15)$$

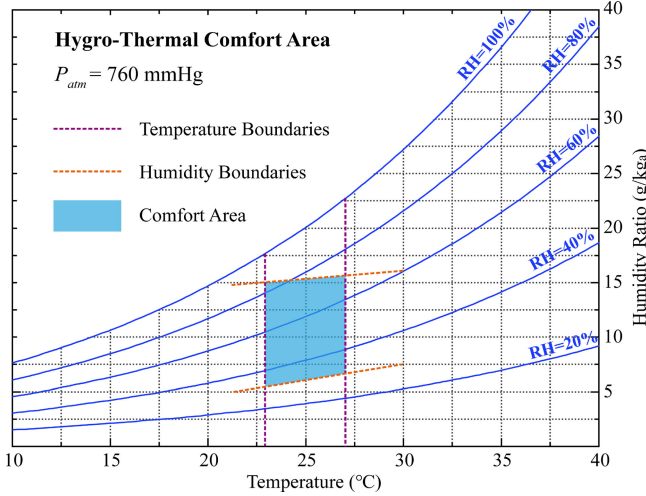


Fig. 2. The hygro-thermal comfort area for building occupants.

where  $p_{ws}(T_a)$  is the saturated vapor pressure at temperature  $T_a$ ;  $P_{atm}$  is the atmospheric pressure;  $k_a$ ,  $k_b$ , and  $k_C$  are the coefficients for different liquids. For water vapor, these values are 8.07131, 1730.63, and 233.426, respectively [34].

Using equations (11)–(15), the temperature and humidity ratio of the supply air can be calculated by assuming the RH of the supply air is 90% [33]. Finally, it is necessary to validate whether the solved humidity ratio is smaller than that of mixed air. If not, the temperature should be recalculated using the humidity ratio of the mixed air.

Modeling the air conditioning process shows that the cooling capacity provided by HVAC systems is a key factor influencing the state of the supply air. Therefore, the next subsection will investigate the relationship between the cooling capacity and the power consumption of HVAC systems.

### C. Model of HVAC Equipment

In HVAC systems, chillers convert electricity into cooling capacity and serve as the primary source of regulation capacity. Cooling capacity is transferred via the chilled water from chillers to cooling coils, where cooling and dehumidification processes occur simultaneously. The cooling capacity provided by HVAC systems can be expressed as follows [19]:

$$Q_{\text{HVAC}}^t = m_{\text{cw}}^t C_{\text{water}} (T_{\text{cwr}}^t - T_{\text{cws}}^t) \quad (16)$$

where  $m_{\text{cw}}^t$  represents the mass flow rate of chilled water;  $C_{\text{water}}$  is the specific heat of water;  $T_{\text{cwr}}^t$  and  $T_{\text{cws}}^t$  indicate the temperature of return and supply chilled water, respectively.

Furthermore, the cooling capacities delivered to different rooms depend on the temperature of the chilled water. Hence, the regulation capacities required for DR can be effectively distributed among rooms through the temperature variations of the chilled water, thus achieving approximately similar levels of thermal discomfort.

Neglecting the time delay in cooling capacity transmission due to pipe length, the cooling capacity can be related to

electric power and the coefficient of performance (COP) as follows:

$$P_{\text{chiller}}^t = \frac{Q_{\text{HVAC}}^t}{\eta_{\text{cop}}^t} \quad (17)$$

where  $P_{\text{chiller}}^t$  is the electric power consumed by chillers;  $\eta_{\text{cop}}^t$  is the COP of chillers, indicating the conversion efficiency from electricity to cooling capacity.

Additionally, the energy consumption of pumps and the cooling tower is proportional to the cooling capacity. Based on the water transfer factor (WTF), their real-time power consumption can be expressed as follows [35]:

$$P_{\text{pump}}^t = \frac{Q_{\text{HVAC}}^t}{WTF_{\text{pump}}} \quad (18)$$

$$P_{\text{tower}}^t = \frac{Q_{\text{HVAC}}^t}{WTF_{\text{tower}}} \quad (19)$$

where  $P_{\text{pump}}^t$  and  $P_{\text{tower}}^t$  are the power of pumps and cooling towers, respectively;  $WTF_{\text{pump}}$  and  $WTF_{\text{tower}}$  are the water transfer factors for pumps and cooling towers, respectively.

These models are developed for HVAC systems operating in cooling mode, primarily focusing on DR potential during the cooling season. They are also applicable to buildings equipped with multiple chillers or HVAC systems. For multiple chillers, the additional dispatch strategy can be employed to coordinate the allocation of cooling capacity. In contrast, multiple HVAC systems can be treated as different subsystems according to their respective cooling zones, which are independently modeled and controlled to explore the feasible regulation region.

## III. HYGRO-THERMAL COMFORT AREA AND AIR DYNAMICS

Building on the HVAC system models, the T&H boundaries of comfort areas are defined in this Section to explore the feasible regulation region. The comfort area with hygro-thermal interaction is established first, followed by the classification of hygro-thermal dynamics of zone air during DR deployment.

### A. Description of Hygro-Thermal Comfort Area During DR

In most HVAC systems, the zone cooling process is actively controlled, with the system continuously adjusting cooling capacity to maintain the temperature around the setpoint [36]. In contrast, dehumidification is a passive process, making it challenging to control humidity separately without additional equipment. Under normal operating conditions, humidity can be maintained within the comfort area. However, DR represents a special operating scenario for HVAC systems, necessitating extra awareness of humidity to ensure hygro-thermal comfort.

Unlike previous work that considered temperature alone, the hygro-thermal comfort emphasizes the varying humidity requirements during DR. The hygro-thermal comfort area constrained by T&H is defined, as shown in Fig. 2.

Firstly, the zone temperature should be limited to the temperature boundaries:

$$T_z^{\min} \leq T_z^t \leq T_z^{\max} \quad (20)$$

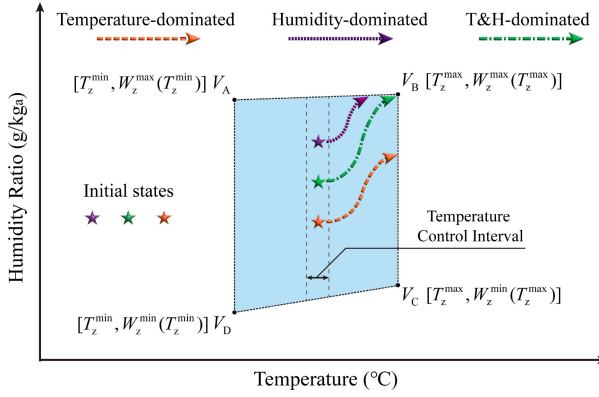


Fig. 3. The hygro-thermal dynamics of zone air when participating in DR.

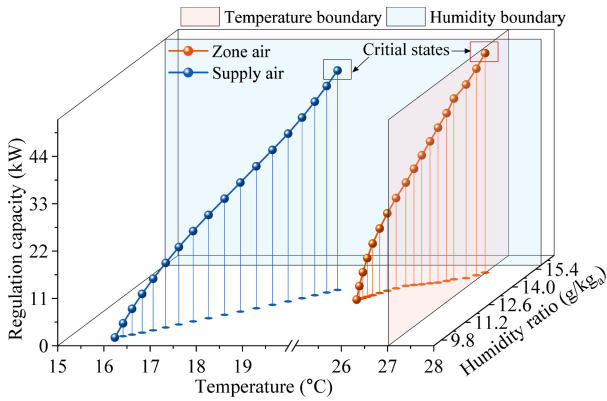


Fig. 4. The T&H dynamics of the zone air and supply air when exploring the feasible regulation region.

where  $T_z^{\min}$  and  $T_z^{\max}$  mirror the acceptable minimum and maximum temperature, respectively.

Similarly, the zone humidity should be limited to humidity boundaries that vary with temperature:

$$W_z^{\min}(T_z^t) \leq W_z^t \leq W_z^{\max}(T_z^t) \quad (21)$$

where  $W_z^{\max}(T_z^t)$  and  $W_z^{\min}(T_z^t)$  represent the maximum and minimum humidity ratios at a given zone temperature  $T_z^t$ , respectively.

As shown in Fig. 3, the comfort area can be determined by 4 vertexes, namely  $V_a$ ,  $V_b$ ,  $V_c$ , and  $V_d$ , whose temperatures and humidity ratios can be expressed as follows:

$$\begin{cases} T_a = T_z^{\min}, W_a = W_z^{\max}(T_z^{\min}) \\ T_b = T_z^{\max}, W_b = W_z^{\max}(T_z^{\max}) \\ T_c = T_z^{\max}, W_c = W_z^{\min}(T_z^{\max}) \\ T_d = T_z^{\min}, W_d = W_z^{\min}(T_z^{\min}) \end{cases} \quad (22)$$

where  $T_a$ ,  $T_b$ ,  $T_c$ , and  $T_d$  are the temperatures at  $V_a$ ,  $V_b$ ,  $V_c$ , and  $V_d$ , respectively;  $W_a$ ,  $W_b$ ,  $W_c$ ,  $W_d$  are the humidity ratios at  $V_a$ ,  $V_b$ ,  $V_c$ , and  $V_d$ , respectively.

On this basis, both varying upper and lower boundaries can be calculated as follows:

$$W_z^{\max}(T_z^t) = W_a + \frac{W_b - W_a}{T_b - T_a} (T_z^t - T_a) \quad (23)$$

$$W_z^{\min}(T_z^t) = W_c + \frac{W_d - W_c}{T_d - T_c} (T_z^t - T_c) \quad (24)$$

The specific values of humidity ratios at 4 vertexes can be determined by setting the RH values. Considering that both T&H affect occupant comfort, the maximum RH is required to decrease with increasing temperature, while the minimum RH remains constant to prevent excessively dry environments. Hence, the RH values at  $V_a$ ,  $V_b$ ,  $V_c$ , and  $V_d$  are set as 85%, 75%, 30%, and 30% in this paper, respectively. It should be noted that these values can be customized according to local climate, individual demands, and other factors.

### B. Classification for Hygro-Thermal Air Dynamics

According to the hygro-thermal comfort area, the subsequent challenge is to determine the maximum regulation power. Traditionally, this power is evaluated based on the temperature differences between initial and final air states. However, the incorporation of humidity introduces a new complexity, as both initial and final air states are characterized by T&H. Worse still, it is difficult to separately describe the T&H dynamics driven by power adjustments.

When HVAC systems operate under normal conditions, zone temperature can be controlled within a narrow range, because the control system actively adjusts the cooling capacity to eliminate temperature deviations. Conversely, passive humidity control makes it challenging to maintain a stable humidity ratio. As shown in Fig. 3, the initial temperature is typically around the preset value, while the humidity ratio exhibits a broader distribution.

Upon DR activation, the zone air transitions from initial states to new steady states over time. The specific variation tendencies of T&H are affected by numerous factors. Under the combined effects of initial states and variation tendencies, the final air states will reach either the temperature or humidity boundary. As a result, the hygro-thermal dynamics of zone air are classified into 3 types: temperature-dominated, humidity-dominated, and T&H-dominated, represented by orange dashed line, purple dotted line, and green dash-dotted line in Fig. 3, respectively.

1) Temperature-dominated: the temperature first reaches or exceeds the temperature boundary.

2) Humidity-dominated: the humidity ratio first reaches or exceeds the humidity boundary.

3) T&H-dominated: the temperature and humidity ratio reach or exceed their corresponding boundaries simultaneously.

Classifying hygro-thermal dynamics helps focus on the primary factor when exploring the maximum power regulation, particularly given the complicated coupling relationships between T&H.

## IV. EXPLORATION OF FEASIBLE REGULATION REGION

The feasible regulation region is explored by determining the operating power of HVAC systems, which precisely positions the zone air at the boundaries of the hygro-thermal comfort area. Firstly, a criterion is proposed to identify the types of hygro-thermal dynamics. Secondly, the steady parameters of HVAC systems during regulation are determined. Finally, the quantitative evaluation for feasible regulation

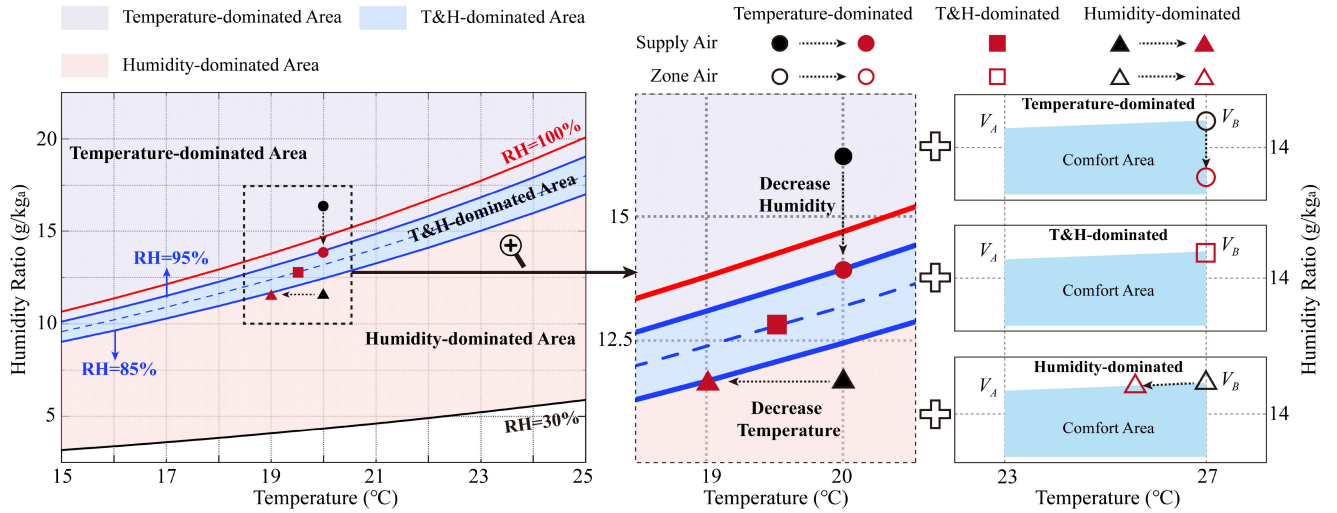


Fig. 5. The criterion for supply air to distinguish the hygro-thermal dynamic and the corresponding states of zone air.

regions is conducted, accompanied by their integration into the Building Automation System (BAS).

#### A. A Criterion for Hygro-Thermal Dynamics During DR

It is essential to identify the critical states of both the zone air and the supply air. As depicted in Fig. 4, these critical states indicate that the T&H of the zone air have reached the boundaries of comfort area, and the corresponding regulation capacity is also at its maximum value. Hence, exploration in feasible regulation regions primarily focuses on determining these critical states of the zone air and the supply air. Due to the coupling characteristics between T&H, it is challenging to determine the final critical states without full knowledge of boundary conditions, except for point-by-point calculation.

To address this, a novel criterion is proposed to identify the specific hygro-thermal dynamics. Taking downward DR as an example, we initially assume that the hygro-thermal dynamic is of the T&H-dominated type. Hence, the T&H of zone air are exactly equal to  $T_B$  and  $W_B$ . Besides, the indoor T&H remains constant, rendering the 2 differential terms  $dT_z^t/dt$  and  $dW_z^t/dt$  in (2) and (8) equal to zero.

The trial solution of sensible load  $Q_{\text{HVAC}}^{\text{s,tri}}$  can be derived as follows:

$$Q_{\text{HVAC}}^{\text{s,tri}} = K_{\text{env}} A_{\text{sf}} (T_{\text{oa}}^t - T_B) + Q_{\text{solar}}^t + Q_{\text{occ}}^t \quad (25)$$

Thus, the trial solutions of the supply air can be obtained by substituting them into (4) and (8):

$$T_{\text{sa}}^{\text{tri}} = T_B - \frac{Q_{\text{HVAC}}^{\text{s,tri}}}{m_{\text{sa}}^t C_{\text{air}}} \quad (26)$$

$$W_{\text{sa}}^{\text{tri}} = W_B - \frac{N_{\text{occ}}^t (\dot{m}_{\text{w,occ}} + \dot{m}_{\text{w,equip}})}{m_{\text{sa}}^t} \quad (27)$$

where  $T_{\text{sa}}^{\text{tri}}$  and  $W_{\text{sa}}^{\text{tri}}$  are the trial solutions of the temperature and humidity ratio of the supply air, respectively.

These trial solutions for the supply air position the zone air at the vertex  $V_B$ . The key to identifying the hygro-thermal dynamics is the RH of the supply air, as shown in Fig. 5.

Typically, the humidity of the supply air is nearly saturated, resulting in an RH of approximately 90%. Allowing for slight fluctuations, the RH interval of [85%, 95%], represented by the blue area, is adopted as the T&H-dominated region. When the states of supply air fall within this area (indicated by the red filled square), the assumption holds that the hygro-thermal dynamic is T&H dominated.

$$85\% \leq RH(T_{\text{sa}}^{\text{tri}}, W_{\text{sa}}^{\text{tri}}) \leq 95\% \quad (28)$$

If the humidity ratio of the supply air falls below the blue area (represented by the black-filled triangle), it indicates that decreasing the temperature is the only way to achieve the 90% RH requirement, as higher humidity levels would result in humidity violations. Accordingly, the states of zone air transition from the black open triangle to the red one. Hence, the hygro-thermal dynamic is classified as the humidity-dominated type.

$$30\% \leq RH(T_{\text{sa}}^{\text{tri}}, W_{\text{sa}}^{\text{tri}}) < 85\% \quad (29)$$

On the contrary, if the humidity ratio is located in the purple area (indicated by the black-filled circle), it suggests that reducing humidity is a viable option to limit the temperature within the boundary while keeping the supply air at 90% RH. Meanwhile, the states of zone air transfer from the black open circle to the red one. Therefore, the hygro-thermal dynamic is the temperature-dominated type. Notably, the purple area encompasses conditions where the RH exceeds 100%, which appears to violate physical constraints. In fact, the trial solution is only an index to identify the hygro-thermal dynamic and will not be used in the following analysis.

$$RH(T_{\text{sa}}^{\text{tri}}, W_{\text{sa}}^{\text{tri}}) > 95\% \quad (30)$$

The trial solutions serve as a criterion for identifying the hygro-thermal dynamics. It should be noted that the final steady states of the zone air need to be recalculated, rather than directly utilizing the trial solutions. Specific calculations are illustrated in the following subsection.

### B. Parameter Determination of Steady Air States During DR

Based on the identified hygro-thermal dynamics, the states of the supply air and zone air should be updated to determine the HVAC system parameters during DR deployment. This ensures accurate information for the exploration of the feasible regulation region.

1) Humidity-dominated type: To avoid humidity constraint violation, the humidity ratio of the supply air cannot be increased. Hence, the temperature should be decreased from the black-filled triangle to the red-filled triangle as shown in Fig. 5.

$$RH(T_{sa}^{DR}, W_{sa}^{DR}) = 85\% \quad (31)$$

$$W_{sa}^{DR} = W_{sa}^{tri} \quad (32)$$

where  $T_{sa}^{DR}$  and  $W_{sa}^{DR}$  are the temperature and humidity ratio of the supply air during DR, respectively.

2) Temperature-dominated type: To maintain the temperature of the supply air, the humidity should be decreased from the black-filled circle to the red-filled circle as shown in Fig. 5.

$$RH(T_{sa}^{DR}, W_{sa}^{DR}) = 95\% \quad (33)$$

$$T_{sa}^{DR} = T_{sa}^{tri} \quad (34)$$

3) T&H-dominated type: The states of the supply air are equal to the trial solutions.

$$T_{sa}^{DR} = T_{sa}^{tri} \quad (35)$$

$$W_{sa}^{DR} = W_{sa}^{tri} \quad (36)$$

In accordance with the updated parameters of the supply air, the states of the zone air also should be recalculated as follows:

$$T_z^{DR} = \frac{m_{sa}^t C_{air} T_{sa}^{DR} + K_{env} A_{sf} T_{oa}^t + Q_{solar}^t + Q_{occ}^t}{m_{sa}^t C_{air} + K_{env} A_{sf}} \quad (37)$$

$$W_z^{DR} = W_{sa}^{DR} + \frac{N_{occ}^t (\dot{m}_{w,occ} + \dot{m}_{w,equip})}{m_{sa}^t} \quad (38)$$

where  $T_z^{DR}$  and  $W_z^{DR}$  represent the final steady states of the zone air during DR, respectively.

### C. Quantitative Evaluation of Feasible Regulation Region

Since the critical parameters of HVAC systems during DR events have been determined, the feasible regulation region can be quantitatively evaluated by calculating the necessary cooling capacity.

The cooling capacity can be obtained by the enthalpy differences between the supply and mixed air. Their enthalpy can be expressed as follows:

$$h_{sa}^{DR} = 1.005T_{sa}^{DR} + (1.84T_{sa}^{DR} + 2500)W_{sa}^{DR} \quad (39)$$

$$h_{ma}^{DR} = 1.005T_{ma}^{DR} + (1.84T_{ma}^{DR} + 2500)W_{ma}^{DR} \quad (40)$$

$$\begin{cases} T_{ma}^{DR} = \frac{m_{ra}^t T_z^{DR} + m_{oa}^t T_{oa}^t}{m_{sa}^t} \\ W_{ma}^{DR} = \frac{m_{ra}^t W_z^{DR} + m_{oa}^t W_{oa}^t}{m_{sa}^t} \end{cases} \quad (41)$$

On this basis, the necessary cooling capacity provided by HVAC systems during DR events can be expressed as follows:

$$Q_{HVAC}^{DR} = m_{sa}^t (h_{sa}^{DR} - h_{ma}^{DR}) \quad (42)$$

Let  $Q_{HVAC}^{\text{steady}}$  denote the baseline cooling capacity under setpoint tracking (i.e., non-DR operation), the maximum reduction in cooling capacity  $\Delta Q_{HVAC}^{\max}$  can be obtained.

$$\Delta Q_{HVAC}^{\max} = Q_{HVAC}^{\text{steady}} - Q_{HVAC}^{DR} \quad (43)$$

The maximum regulation power of HVAC systems can be derived from the 3 primary components associated with variations in cooling capacity: chillers, water pumps, and cooling towers.

$$\Delta P_{HVAC}^{\max} = \frac{\Delta Q_{HVAC}^{\max}}{\eta_{cop}^t} + \frac{\Delta Q_{HVAC}^{\max}}{WTF_{pump}} + \frac{\Delta Q_{HVAC}^{\max}}{WTF_{tower}} \quad (44)$$

where  $\Delta P_{HVAC}^{\max}$  is the maximum regulation power of HVAC systems;  $\Delta Q_{HVAC}^{\max}/\eta_{cop}^t$ ,  $\Delta Q_{HVAC}^{\max}/WTF_{pump}$ , and  $\Delta Q_{HVAC}^{\max}/WTF_{tower}$  indicate the maximum regulation power of chillers, pumps, and cooling towers, respectively.

### D. Integration of the Feasible Regulation Region Into BAS

The feasible regulation region defines the available flexibility throughout the day, which can be integrated into the BAS for optimal utilization. The hygro-thermal comfort of occupants can be maintained when the regulation power remains within the defined region.

Building HVAC systems can participate in DR programs through various methods, such as market bidding and regulation contracts [36]. Therefore, the BAS needs to submit the regulation capacity to power system operators or aggregators at specific times. After optimization and dispatch by power systems, the specific DR capacity and corresponding schedule are sent to the BA. The BAS then adjusts the operating power of HVAC systems to deliver DR services.

In addition to DR services, the remaining flexibility can be further exploited. For instance, it can be treated and dispatched as virtual energy storage, aimed at improving energy efficiency and reducing operational costs. Specifically, the BAS can adjust the power consumption of HVAC systems based on real-time electricity prices or PV generation.

Through this two-stage utilization, the HVAC flexibility can support the supply-demand balance of power systems while optimizing the operational performance of the building.

## V. CASE STUDY

Numerical simulations are conducted using realistic data in this section. The feasible regulation region is explored, demonstrating the advantages of incorporating humidity. Then, the accuracy of the proposed method is analyzed. Finally, the impacts of multiple factors on the operation and flexibility of HVAC systems are investigated.

### A. Parameter Settings

Detailed information on the test building and HVAC systems is provided in TABLE I. Among them, the heat transfer coefficient and thermal capacity of the zone are estimated based on extensive operational data, addressing challenges in parameter acquisition. Setpoint preferences are collected from over 3,000 occupants to define the comfort area. The

TABLE I  
INFORMATION ON THE BUILDING AND HVAC SYSTEMS

Symbols	Definitions/Descriptions	Values	Unit
$A_{sf}$	Surface area of the building	6,600	$\text{m}^2$
$K_{env}$	Heat transfer coefficient	8	$\text{W}/(\text{m}^2 \cdot ^\circ\text{C})$
$C_z$	Thermal capacity of the zone	44,305	$\text{kJ}/^\circ\text{C}$
$\gamma_w$	Window-to-wall ratio	0.3	\
$\gamma_{SHGC}$	Solar heat gain coefficient	0.2	\
$N_{occ}^{\max}$	Maximum number of occupants	1,200	\
$\rho_{air}$	Density of air	1.205	$\text{kg}/\text{m}^3$
$C_{air}$	Specific heat of air	1.005	$\text{kJ}/(\text{kg} \cdot ^\circ\text{C})$
$Q_{occ}$	Heat release per occupant	70	W
$Q_{equip}$	Heat release by equipment per occupant	100	W
$m_{w,occ}$	Humidity release per occupant	0.0464	$\text{g}/\text{s}$
$m_{w,equip}$	Humidity release by equipment per occupant	0.0139	$\text{g}/\text{s}$
$\eta'_{cop}$	COP of chillers	5	\
$WTF_{pump}$	Water transfer factor of pumps	60	\
$WTF_{tower}$	Water transfer factor of cooling tower	55	\
$m_{sa}^{\max}$	Maximum mass of supply air	120	$\text{kg}/\text{s}$

temperature setpoint is set at  $25^\circ\text{C}$ . The hygro-thermal comfort area is determined by 4 vertexes:  $V_A(23^\circ\text{C}, 15.02\text{g/kg}_A)$ ,  $V_B(27^\circ\text{C}, 15.71\text{g/kg}_A)$ ,  $V_C(27^\circ\text{C}, 6.64\text{g/kg}_A)$ , and  $V_D(23^\circ\text{C}, 5.22\text{g/kg}_A)$ . The COP of chillers, as well as the water transfer factors of pumps and cooling towers, are regarded as constant during operation.

The mass flow rate of the supply air is proportional to the real-time number of occupants, as fan coil units are activated or deactivated according to occupant activities.

$$m_{sa}^t = 0.25 \cdot m_{sa}^{\max} + 0.75 \cdot m_{sa}^{\max} \left(1 - N_{occ}^t / N_{occ}^{\max}\right) \quad (45)$$

where  $m_{sa}^{\max}$  is the maximum air flow rate of supply air;  $N_{occ}^{\max}$  is the maximum number of occupants within the building.

To ensure sufficient fresh air, the percentage of the mass flow rate of outdoor air remains constant:

$$m_{ma}^t / m_{oa}^t = 8 \quad (46)$$

The Random Forest approach is employed to infer the number of occupants according to Wi-Fi connections, without requiring additional equipment [30]. This approach establishes a relationship between occupant numbers and Wi-Fi connections, which is cost-effective for most public buildings. The inferred occupant numbers are used to reveal occupant activities, and the global horizontal irradiance (GHI) is utilized to indicate the real-time solar radiation, as illustrated in Fig. 6 (a). The ambient temperature and humidity ratio are sourced from a typical summer day [38], [39], as shown in Fig. 6 (b). Note that the variations of humidity ratios are not remarkable, while the RH has significant differences due to temperature variations. For instance, RH values are 60% and 85% at 14:00 and 23:00, respectively.

#### B. Exploration of Feasible Regulation Region

Most HVAC systems actively control the zone temperature to minimize deviations by adjusting its cooling capacity. As

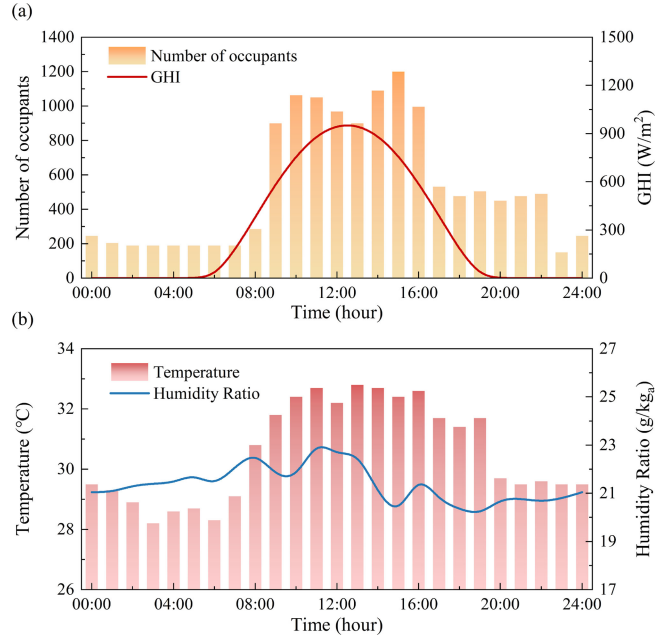


Fig. 6. Simulation parameters: (a) occupant activities and GHI; (b) ambient temperature and humidity ratio.

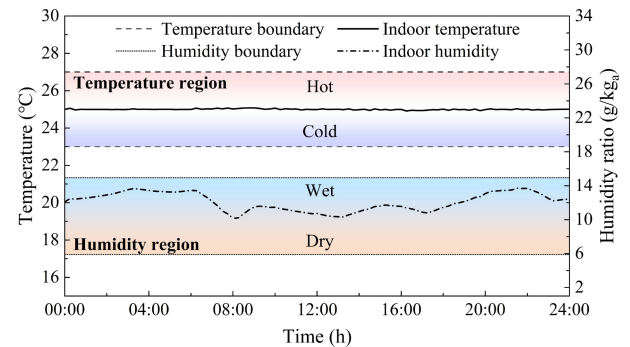


Fig. 7. The temperature and humidity ratio profiles of zone air throughout the whole-day operation.

illustrated in Fig. 7, the zone temperature can be maintained at  $25^\circ\text{C}$  throughout the day. However, due to passive humidity control, humidity ratios fluctuate frequently under the influence of multiple factors.

Specifically, humidity ratios are well controlled during 08:00-18:00, maintaining levels near the center of the comfort range. In contrast, zone humidity ratios are much higher at night, with the maximum value reaching  $13.69\text{g/kg}_a$ , an increase of 35.7% compared to the minimum value. Given that outdoor humidity ratios exhibit only slight variations, the reduced dehumidification capacity of HVAC systems is likely the primary cause. As solar radiation and occupant activity decrease, HVAC cooling capacities decrease at night, reducing the latent loads available for dehumidification.

Using the proposed criterion, the specific hygro-thermal dynamics of upward and downward regulations are first identified. As shown in Fig. 8, the temperature-dominated, T&H-dominated, and humidity-dominated are represented by purple, blue, and red spheres, respectively. On this basis, the

TABLE II  
REGULATION CAPACITY RATIOS FOR DIFFERENT  
HYGRO-THERMAL DYNAMICS

Hygro-thermal dynamics	Temperature-dominated	T&H-dominated	Humidity-dominated
Average values	17.80%	33.82%	30.52%
Maximum values	36.79%	44.31%	38.01%
Minimum values	12.39%	23.51%	23.47%

feasible regulation region of HVAC systems is explored and represented by the blue area.

In upward regulation, the hygro-thermal dynamics are predominantly temperature-dominated, as the humidity ratio rarely violates the lower humidity constraint in hot and humid conditions. As a result, the regulation capacity ratio during the day is lower than that at night due to daily temperature variations, as depicted in Fig. 9.

By contrast, downward regulation is more representative, with hygro-thermal dynamics influenced by varying outdoor and indoor factors, exhibiting distinct results throughout the day. Therefore, the following analysis mainly focuses on this aspect. When humidity ratios approach the upper boundary, the hygro-thermal dynamic is of the humidity-dominated type. Conversely, the hygro-thermal dynamic shifts to temperature-dominated when humidity ratios are centered within the humidity region during 07:30–18:30. Hence, the T&H-dominated type consistently appears as a transitional state between temperature-dominated and humidity-dominated types.

Further regulation capacity ratios reveal that their peak values consistently occur when the hygro-thermal dynamic is T&H-dominated. The maximum regulation capacity ratios reach 40.97% and 44.31% at 06:30 and 23:00, respectively. To assess the impacts of the hygro-thermal dynamic, the average, maximum, and minimum values of regulation capacity ratios are calculated, as shown in TABLE II.

The results demonstrate consistent characteristics across different indexes. The T&H-dominated type consistently achieves the highest regulation capacity ratios, while the temperature-dominated type exhibits the lowest regulation capacity. It is reasonable for the T&H-dominated type to realize the maximum values by fully utilizing the T&H variations. In contrast, the temperature-dominated type experiences significant occupant activities and solar radiation, leading to noticeable temperature growth during DR events. Thus, the average regulation capacity ratio is only 17.8%. The humidity-dominated type achieves regulation capacities comparable to those of the T&H-dominated type, primarily due to reduced humidity contributions from occupants and equipment.

The sensible loads and latent loads are also illustrated in Fig. 9. The maximum and minimum percentages of latent loads are 48.73% and 32.11%, respectively. As mentioned in [23], latent loads contribute significantly to total cooling loads, particularly in high-humidity areas. However, previous studies have often overlooked the latent loads.

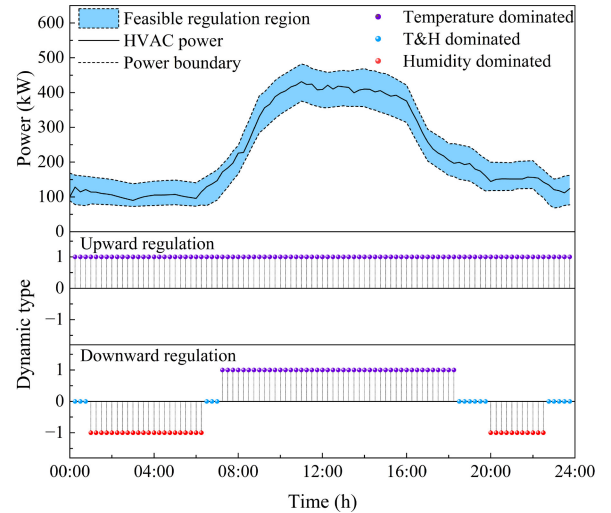


Fig. 8. The feasible regulation regions and corresponding hygro-thermal dynamic types of HVAC systems.

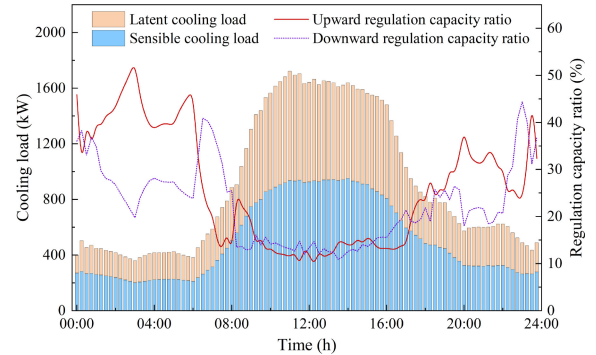


Fig. 9. The specific sensible and latent loads and the corresponding regulation capacity ratio.

### C. The Impact of Humidity on HVAC Regulation

Most existing literature evaluates the regulation potential of HVAC systems solely based on zone temperatures, often overlooking the critical role of humidity. Recognizing that humidity impacts occupant comfort and consequently influences the feasible regulation region capacity of HVAC systems, scenarios with and without humidity consideration are conducted to illustrate its effects.

Fig. 10 shows the evaluated regulation capacities at different time instants. By adjusting the power of HVAC systems based on the corresponding results, the states of zone air are further analyzed: Fig. 11 (a) exhibits the temperature and humidity ratio, and Fig. 11 (b) indicates the apparent temperature. The apparent temperature reflects the combined effects of T&H on occupant comfort, which can be calculated as follows [40]:

$$T_{at} = T + 0.33 \times RH_a \times 6.105 \times e^{\frac{17.27T}{237.7+T}} - 4 \quad (47)$$

where  $T_{at}$  and  $T$  are the apparent and dry-bulb temperature.

When comparing the 2 scenarios, the most significant differences occur when hygro-thermal dynamics are dominated by humidity, while they remain similar under other conditions.

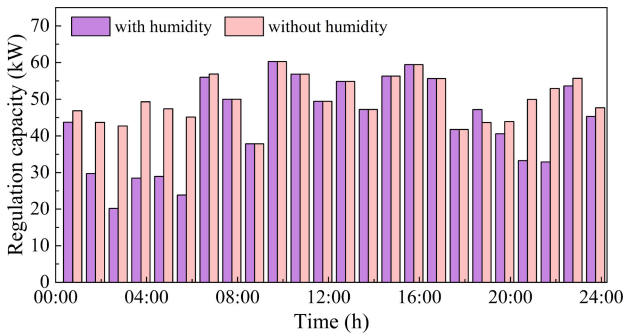


Fig. 10. Comparison of regulation capacity between scenarios with and without humidity consideration.

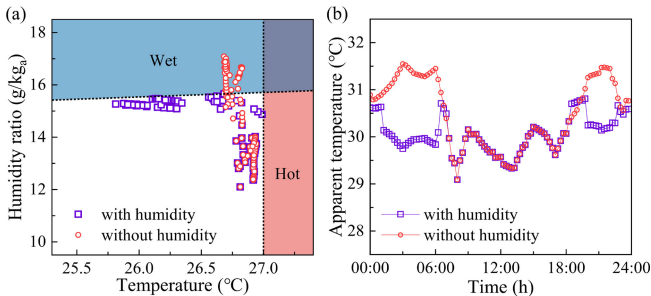


Fig. 11. Comparison of zone air between scenarios with and without humidity consideration. (a) Temperature and humidity ratio; (b) Apparent temperature.

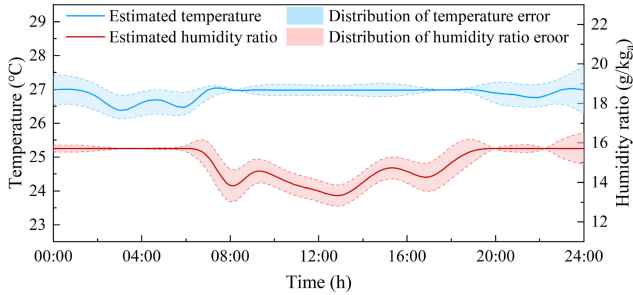


Fig. 12. The error distributions of the estimated T&H during DR deployment.

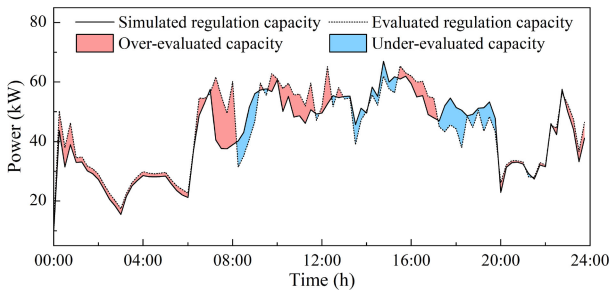


Fig. 13. Comparisons between simulated and evaluated regulation capacities.

Specifically, incorporating humidity limits further regulation even when the temperature does not reach the boundary. To prevent thermal discomfort caused by high humidity levels, the temperature is constrained to approximately 25.5°C under

TABLE III  
ESTIMATED DEVIATIONS OF T&H

Estimated deviations	Temperature	Humidity
Average absolute values	0.254°C	0.437g/kg <sub>a</sub>
Maximum values	0.704°C	0.903g/kg <sub>a</sub>
Minimum values	0.007°C	0.007g/kg <sub>a</sub>

the most extreme conditions, representing a minor increase from the setpoint. Conversely, neglecting humidity leads to significant violations of humidity constraint, with the highest humidity ratio exceeding 17g/kg<sub>a</sub>, as shown in Fig. 11 (a). Moreover, the variations in apparent temperature are smaller throughout the operation when humidity is considered. A more uniform sensible temperature helps prevent distinct comfort differences under varying conditions and aids in identifying the stable comfort area. Otherwise, occupants may frequently adjust their temperature preferences due to fluctuating climate conditions.

#### D. Performance Analysis of the Proposed Criterion

To validate the accuracy of the proposed criterion, the errors between estimated and actual values are analyzed. Estimated temperature and humidity ratio are calculated using equations (37)–(38). By holding other parameters constant, the explored maximum regulation capacity is introduced into a 1-hour operation to obtain simulated values, as illustrated in Fig. 12.

Temperature errors are smaller when the hygro-thermal dynamics are temperature-dominated, while humidity errors are minimized in humidity-dominated conditions. Throughout the day, estimation accuracy for T&H often exhibits contradictory features, complicating accurate simultaneous estimations. The allocation of sensible and latent loads is influenced by multiple factors, indicating that even slight deviations in any factor can affect the original allocation. Additionally, errors arising from approximation during estimation are unavoidable. For instance, deriving the temperature and humidity ratio from the enthalpy of air constitutes a primary approximation.

Despite these challenges, most temperature and humidity ratio errors fall within narrow ranges, as shown in TABLE III, suggesting that their impacts on hygro-thermal comfort may not be significant compared to other uncertainties. Moreover, nearly all identifications of hygro-thermal dynamics are accurate, demonstrating the effectiveness of the proposed criterion in identifying hygro-thermal dynamics.

In addition to analyzing the states of zone air, the accuracy of regulation capacity is further examined. The operating power of HVAC systems, which positions the zone air at the boundaries of the comfort area, is simulated to determine the actual regulation capacities by calculating its differences from normal operating power. As shown in Fig. 13, regulation capacity deviations during the daytime are significantly higher than those at night. When combined with hygro-thermal dynamics, it is evident that accuracy is less affected by the temperature-dominated type, as evaluated and simulated values nearly overlap. However, the T&H-dominated and humidity-dominated types significantly impact the accuracy of evaluated

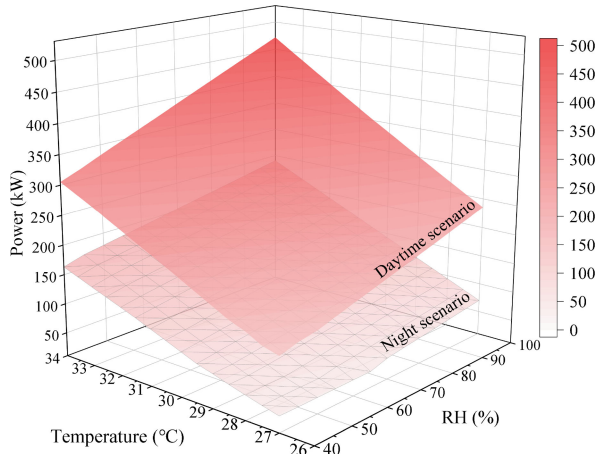


Fig. 14. The impacts of T&H on operating power of HVAC systems.

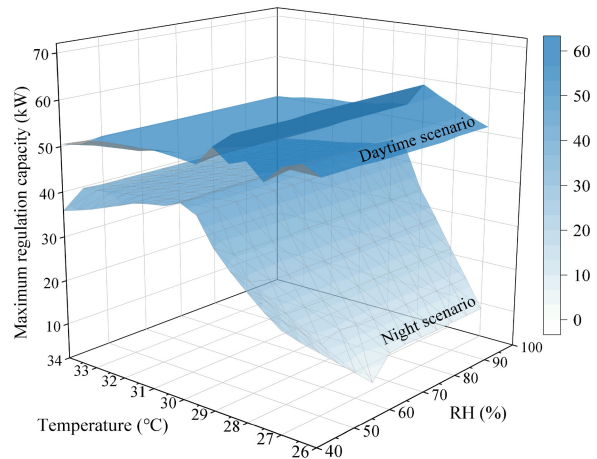


Fig. 15. The impacts of T&H on regulation capacity of HVAC systems.

TABLE IV  
SIMULATION PARAMETERS OF THE DAYTIME AND NIGHT SCENARIOS

Parameters	Daytime scenario	Night scenario
Temperature ranges	[27°C, 34°C]	[27°C, 34°C]
RH ranges	[40%, 100%]	[40%, 100%]
Number of occupants	1080	150
GHI	880 W/m <sup>2</sup>	0

results, with severe deviations occurring at the transition periods (e.g., 21.1kW at 07:30 and 12.5kW at 18:30). Despite these, other deviations remain acceptable, which are consistent with the results of zone air.

These findings underscore the complex interactions between T&H, posing a challenge to accurately exploring the feasible regulation region while maintaining hygro-thermal comfort.

#### E. Operating Power and Feasible Regulation Region Analysis Under Different Conditions

The operating power and the maximum regulation power capacity of HVAC systems are first analyzed under daytime and night scenarios, as shown in TABLE IV.

Other parameters, such as occupants and GHI, are set to match conditions at 11:00 and 22:00, respectively. In the daytime scenario, HVAC systems are temperature-dominated, while they are humidity-dominated type in the nighttime scenario according to their original conditions. However, variations in ambient T&H can alter hygro-thermal dynamics. The simulation steps are set as 0.5°C for temperature and 5% for RH, respectively.

The operating power for the two scenarios is depicted in Fig. 14. Both temperature and RH increases contribute to higher operating power. At lower temperatures, RH increases have a relatively minor impact on operating power. For instance, as RH grows from 40% to 100%, the operating power increases by 106kW (daytime) and 34kW (nighttime) at 27°C. In contrast, at 36°C, the operating power increases by 167 kW (daytime) and 77kW (nighttime) under the same RH change. Additionally, occupant activities and solar radiation significantly influence the operating power. Under identical temperature and RH conditions, the operating power in the daytime scenario is noticeably higher than that in the night scenario.

Furthermore, the characteristics of maximum regulation capacity are investigated in Fig. 15, showing distinct impacts of outdoor T&H on these 2 scenarios. In the daytime scenario, maximum regulation capacities are stable, slightly affected by outdoor T&H variations. Temperature has a more pronounced effect than RH on the feasible regulation region, primarily because most hygro-thermal dynamics are temperature-dominated. Initially, the maximum regulation capacity grows with rising temperature, peaking at 58.6kW at 29°C, then gradually decreases and remains stable despite further temperature increases.

In the nighttime scenario, the hygro-thermal dynamics do not consistently follow the temperature-dominated pattern. At lower temperatures, the dynamic is humidity-dominated, leading to decreased maximum regulation capacity as RH rises. As the temperature grows, the dynamics gradually shift to temperature-dominated, and the maximum regulation capacity grows rapidly from approximately 10kW to around 40kW. Once temperatures exceed 30°C, the maximum regulation capacities exhibit characteristics similar to the daytime scenario, as dynamics convert to the temperature-dominated. These results reveal that outdoor T&H have significant impacts on the operating power and hygro-thermal dynamics of HVAC systems, leading to distinct characteristics in the maximum regulation capacities.

In addition, the feasible regulation region exhibits intertemporal coupling characteristics, influenced by DR deployment and various dynamic factors. Specifically, 80% of the maximum regulation capacity is allocated to HVAC systems between 12:00 and 13:00. As shown in Fig. 16, the operating power of HVAC systems declines to provide DR services. Hence, the available regulation capacity drops from approximately 55kW to 10kW, as the indoor T&H increase. After DR deployment, both the operating power and regulation capacity gradually recover to their normal states with minor fluctuations. These results suggest that the proposed method effectively captures

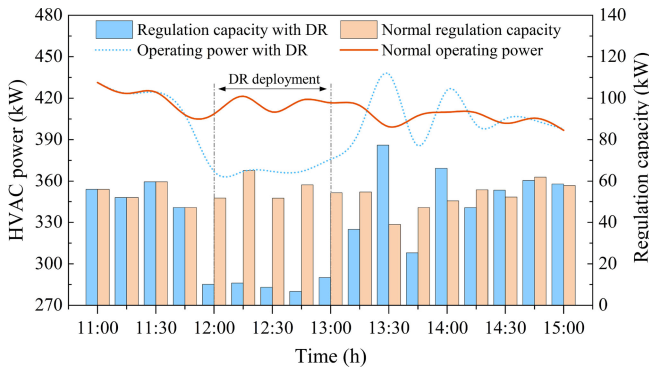


Fig. 16. The impacts of DR deployment on regulation capacities.

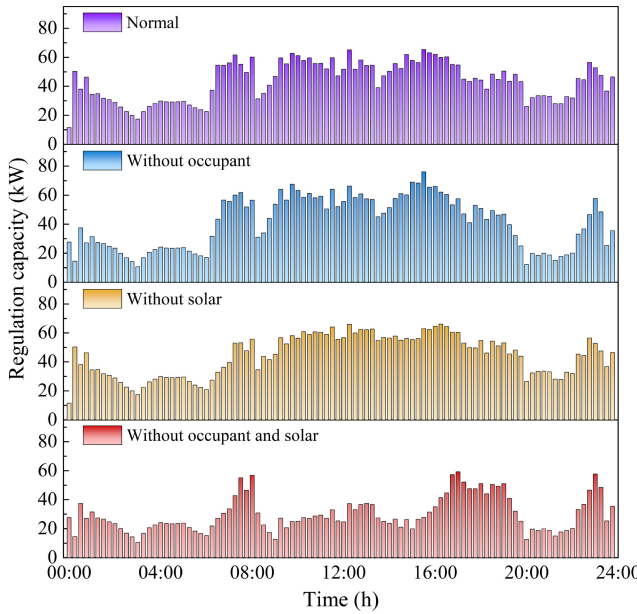


Fig. 17. The impacts of occupant and solar on regulation capacities.

real-time variations, enabling accurate exploration of the feasible regulation region based on current states.

Finally, the impacts of occupant activities and solar radiation on regulation capacity are investigated by isolating their effects, as illustrated in Fig. 17. Regulation capacity is evaluated under 3 scenarios: without occupants, without solar radiation, and without both. Excluding occupant influence notably decreases regulation capacity at night but remains relatively unchanged during the day, except for a few instances. The results further underscore the importance of accurately determining occupant numbers. In this study, occupant numbers are inferred from Wi-Fi connections, which is suitable for those buildings with regular occupancy patterns and consistent Wi-Fi availability. For environments characterized by transient populations and variable device connections, alternative methods, such as image recognition and infrared-based sensors, should be employed to ensure accuracy.

Conversely, setting solar radiation to zero increases lower regulation capacity values while higher values keep stable

in the daytime, leading to more consistent performance. Regulation capacity remains unchanged at night without solar radiation. However, removing both occupant activities and solar radiation sharply decreases regulation capacity. These findings highlight the complex impacts of multiple factors, making it challenging to assess their individual effects on regulation capacity.

## VI. CONCLUSION

This study explores the feasible regulation region of HVAC systems within hygro-thermal comfort by developing a comprehensive model and proposing a criterion to identify critical factors. The case study results validate that both T&H affect the feasible regulation region. The proposed criterion effectively identifies the specific type of hygro-thermal dynamics, facilitating an accurate evaluation of the maximum regulation capacity. Moreover, the impacts of multiple factors are investigated, including *i*) both T&H are proportional to the HVAC operating power; *ii*) the hygro-thermal dynamic type is a critical factor influencing the feasible regulation region; *iii*) multiple varying factors exhibit coupling effects on the feasible regulation region. These findings underscore the importance and necessity of incorporating humidity into the feasible regulation region exploration. However, more data is required to support accurate exploration, which may limit practical implementations. For instance, the inferred occupant numbers may be unreliable, as the Wi-Fi connection-based method is influenced by device types and user behaviors across various buildings.

Based on this research, future work will address potential challenges in the application of large-scale buildings, to achieve the scalability of various buildings with different parameters. Additionally, efforts will focus on real-time active humidity control and its coordination with regulation region evaluation to enhance hygro-thermal comfort.

## REFERENCES

- [1] H. Zhang, X. Hu, Z. Hu, and S. J. Moura, "Sustainable plug-in electric vehicle integration into power systems," *Nat. Rev. Electr. Eng.*, vol. 1, no. 1, pp. 35–52, Jan. 2024, doi: [10.1038/s44287-023-00004-7](https://doi.org/10.1038/s44287-023-00004-7).
- [2] J. Wang et al., "Inherent spatiotemporal uncertainty of renewable power in China," *Nat. Commun.*, vol. 14, no. 1, p. 5379, Sep. 2023, doi: [10.1038/s41467-023-40670-7](https://doi.org/10.1038/s41467-023-40670-7).
- [3] W. Xia, Z. Ren, H. Qin, and Z. Dong, "A coordinated operation method for networked hydrogen-power-transportation system," *Energy*, vol. 296, Jun. 2024, Art. no. 131026, doi: [10.1016/j.energy.2024.131026](https://doi.org/10.1016/j.energy.2024.131026).
- [4] J. Liu et al., "Defining and applying an electricity demand flexibility benchmarking metrics framework for grid-interactive efficient commercial buildings," *Advances in Applied Energy*, vol. 8, Dec. 2022, Art. no. 100107, doi: [10.1016/j.adapen.2022.100107](https://doi.org/10.1016/j.adapen.2022.100107).
- [5] K. Wang et al., "Embedding P2P transaction into demand response exchange: A cooperative demand response management framework for IES," *Appl. Energy*, vol. 367, Aug. 2024, Art. no. 123319, doi: [10.1016/j.apenergy.2024.123319](https://doi.org/10.1016/j.apenergy.2024.123319).
- [6] S. Xia, L. Cai, M. Tong, T. Wu, P. Li, and X. Gao, "Regulation flexibility assessment and optimal aggregation strategy of greenhouse loads in modern agricultural parks," *Protect. Control Modern Power Syst.*, vol. 9, no. 3, pp. 98–111, May 2024, doi: [10.23919/PCMP.2023.000025](https://doi.org/10.23919/PCMP.2023.000025).
- [7] G. Pinto, Z. Wang, A. Roy, T. Hong, and A. Capozzoli, "Transfer learning for smart buildings: A critical review of algorithms, applications, and future perspectives," *Adv. Appl. Energy*, vol. 5, Feb. 2022, Art. no. 100084, doi: [10.1016/j.adapen.2022.100084](https://doi.org/10.1016/j.adapen.2022.100084).

- [8] Z. Zhang, H. Hui, and Y. Song, "Response capacity allocation of air conditioners for peak-valley regulation considering interaction with surrounding microclimate," *IEEE Trans. Smart Grid*, vol. 16, no. 2, pp. 1155–1167, Mar. 2025, doi: [10.1109/TSG.2024.3482361](https://doi.org/10.1109/TSG.2024.3482361).
- [9] Y. Mu et al., "A data-driven rolling optimization control approach for building energy systems that integrate virtual energy storage systems," *Appl. Energy*, vol. 346, Sep. 2023, Art. no. 121362, doi: [10.1016/j.apenergy.2023.121362](https://doi.org/10.1016/j.apenergy.2023.121362).
- [10] N. Lu, "An evaluation of the HVAC load potential for providing load balancing service," *IEEE Trans. Smart Grid*, vol. 3, no. 3, pp. 1263–1270, Sep. 2012, doi: [10.1109/TSG.2012.2183649](https://doi.org/10.1109/TSG.2012.2183649).
- [11] F. Bunning, P. Heer, R. S. Smith, and J. Lygeros, "Increasing electrical reserve provision in districts by exploiting energy flexibility of buildings with robust model predictive control," *Adv. Appl. Energy*, vol. 10, Jun. 2023, Art. no. 100130, doi: [10.1016/j.adapen.2023.100130](https://doi.org/10.1016/j.adapen.2023.100130).
- [12] N. Qi et al., "Smart meter data-driven evaluation of operational demand response potential of residential air conditioning loads," *Appl. Energy*, vol. 279, Dec. 2020, Art. no. 115708, doi: [10.1016/j.apenergy.2020.115708](https://doi.org/10.1016/j.apenergy.2020.115708).
- [13] T. Qi, C. Ye, H. Hui, and Y. Zhao, "Fast frequency regulation utilizing non-aggregate thermostatically controlled loads based on edge intelligent terminals," *IEEE Trans. Smart Grid*, vol. 15, no. 4, pp. 3571–3584, Jul. 2024, doi: [10.1109/TSG.2023.3346467](https://doi.org/10.1109/TSG.2023.3346467).
- [14] P. Yu, H. Zhang, and Y. Song, "Adaptive tie-line power smoothing with renewable generation based on risk-aware reinforcement learning," *IEEE Trans. Power Syst.*, vol. 39, no. 6, pp. 6819–6832, Nov. 2024, doi: [10.1109/TPWRS.2024.3379513](https://doi.org/10.1109/TPWRS.2024.3379513).
- [15] Q. Xie et al., "Use of demand response for voltage regulation in power distribution systems with flexible resources," *IET Gener. Transm. Distrib.*, vol. 14, no. 5, pp. 883–892, 2020, doi: [10.1049/iet-gtd.2019.1170](https://doi.org/10.1049/iet-gtd.2019.1170).
- [16] D. Zhang et al., "Multi-objective control of residential HVAC loads for balancing the user's comfort with the frequency regulation performance," *IEEE Trans. Smart Grid*, vol. 13, no. 5, pp. 3546–3557, Sep. 2022, doi: [10.1109/TSG.2022.3171847](https://doi.org/10.1109/TSG.2022.3171847).
- [17] T. Qi, H. Hui, and Y. Song, "Chance constrained economic dispatch of central air conditionings in large-scale commercial buildings considering demand response," *Energy Build.*, vol. 320, Jul. 2024, Art. no. 114607, doi: [10.1016/j.enbuild.2024.114607](https://doi.org/10.1016/j.enbuild.2024.114607).
- [18] T. Jiang, P. Ju, C. Wang, H. Li, and J. Liu, "Coordinated control of air-conditioning loads for system frequency regulation," *IEEE Trans. Smart Grid*, vol. 12, no. 1, pp. 548–560, Jan. 2021, doi: [10.1109/TSG.2020.3022010](https://doi.org/10.1109/TSG.2020.3022010).
- [19] K. Xie et al., "Modeling and control of central air conditionings for providing regulation services for power systems," *Appl. Energy*, vol. 315, Jun. 2022, Art. no. 119035, doi: [10.1016/j.apenergy.2022.119035](https://doi.org/10.1016/j.apenergy.2022.119035).
- [20] M. Song, C. Gao, S. Ma, J. Meng, and K. Chen, "Distributed scheduling of HVACs based on transactive energy and ADMM," *Appl. Energy*, vol. 325, Nov. 2022, Art. no. 119831, doi: [10.1016/j.apenergy.2022.119831](https://doi.org/10.1016/j.apenergy.2022.119831).
- [21] H. Hui et al., "A transactive energy framework for inverter-based HVAC loads in a real-time local electricity market considering distributed energy resources," *IEEE Trans. Ind. Informat.*, vol. 18, no. 12, pp. 8409–8421, Dec. 2022, doi: [10.1109/TII.2022.3149941](https://doi.org/10.1109/TII.2022.3149941).
- [22] H.-C. Zhu, C. Ren, and S.-J. Cao, "Fast prediction for multi-parameters (concentration, temperature and humidity) of indoor environment towards the online control of HVAC system," *Build. Simul.*, vol. 14, no. 3, pp. 649–665, Jun. 2021, doi: [10.1007/s12273-020-0709-z](https://doi.org/10.1007/s12273-020-0709-z).
- [23] N. S. Raman, K. Devaprasad, B. Chen, H. A. Ingle, and P. Barooah, "Model predictive control for energy-efficient HVAC operation with humidity and latent heat considerations," *Appl. Energy*, vol. 279, Dec. 2020, Art. no. 115765, doi: [10.1016/j.apenergy.2020.115765](https://doi.org/10.1016/j.apenergy.2020.115765).
- [24] Y. Jiang, S. Zhu, Q. Xu, B. Yang, and X. Guan, "Hybrid modeling-based temperature and humidity adaptive control for a multi-zone HVAC system," *Applied Energy*, vol. 334, Mar. 2023, Art. no. 120622, doi: [10.1016/j.apenergy.2022.120622](https://doi.org/10.1016/j.apenergy.2022.120622).
- [25] J. Yuan, Z. Xiao, X. Chen, Z. Lu, J. Li, and W. Gang, "A temperature & humidity setback demand response strategy for HVAC systems," *Sustain. Cities Soc.*, vol. 75, Dec. 2021, Art. no. 103393, doi: [10.1016/j.scs.2021.103393](https://doi.org/10.1016/j.scs.2021.103393).
- [26] ANSI/ASHRAE 55-2023: *Thermal Environmental Conditions for Human Occupancy*, Amer. Soc. Heating, Refrig. Air-Condition. Eng., Atlanta, GA, USA, 2023.
- [27] S. Kumar, J. Mathur, S. Mathur, M. K. Singh, and V. Loftness, "An adaptive approach to define thermal comfort zones on psychrometric chart for naturally ventilated buildings in composite climate of India," *Build. Environ.*, vol. 109, pp. 135–153, Nov. 2016, doi: [10.1016/j.buildenv.2016.09.023](https://doi.org/10.1016/j.buildenv.2016.09.023).
- [28] S. Schiavon, T. Hoyt, and A. Piccioli, "Web application for thermal comfort visualization and calculation according to ASHRAE standard 55," *Build. Simul.*, vol. 7, no. 4, pp. 321–334, Aug. 2014, doi: [10.1007/s12273-013-0162-3](https://doi.org/10.1007/s12273-013-0162-3).
- [29] J. A. Davis and D. W. Nutter, "Occupancy diversity factors for common university building types," *Energy and Buildings*, vol. 42, no. 9, pp. 1543–1551, Sep. 2010, doi: [10.1016/j.enbuild.2010.03.025](https://doi.org/10.1016/j.enbuild.2010.03.025).
- [30] Z. Wang, T. Hong, M. A. Piette, and M. Pritoni, "Inferring occupant counts from Wi-Fi data in buildings through machine learning," *Building and Environment*, vol. 158, pp. 281–294, Jul. 2019, doi: [10.1016/j.buildenv.2019.05.015](https://doi.org/10.1016/j.buildenv.2019.05.015).
- [31] S. Goyal and P. Barooah, "A method for model-reduction of non-linear thermal dynamics of multi-zone buildings," *Energy Build.*, vol. 47, pp. 332–340, Apr. 2012, doi: [10.1016/j.enbuild.2011.12.005](https://doi.org/10.1016/j.enbuild.2011.12.005).
- [32] Y. A. Cengel and M. A. Boles, *Thermodynamics: An Engineering Approach*, 8th ed. New York, NY, USA: McGraw-Hill Educ., 2015.
- [33] Z. Ding et al., "On-site measurement and simulation investigation on condensation dehumidification and desiccant dehumidification in Hong Kong," *Energy Build.*, vol. 254, Jan. 2022, Art. no. 111560, doi: [10.1016/j.enbuild.2021.111560](https://doi.org/10.1016/j.enbuild.2021.111560).
- [34] D. Roizard, "Antoine equation," in *Encyclopedia of Membranes*, E. Drioli and L. Giorno, Eds., Berlin, Germany: Springer, 2014, pp. 1–3, doi: [10.1007/978-3-642-40872-4\\_26-1](https://doi.org/10.1007/978-3-642-40872-4_26-1).
- [35] B. Gao, X. Zhu, X. Yang, Y. Yuan, N. Yu, and J. Ni, "Operation performance test and energy efficiency analysis of ground-source heat pump systems," *J. Build. Eng.*, vol. 41, Sep. 2021, Art. no. 102446, doi: [10.1016/j.jobe.2021.102446](https://doi.org/10.1016/j.jobe.2021.102446).
- [36] Z. Afroz, G. Shafullah, T. Urmee, and G. Higgins, "Modeling techniques used in building HVAC control systems: A review," *Renew. Sustain. Energy Rev.*, vol. 83, pp. 64–84, Mar. 2018, doi: [10.1016/j.rser.2017.10.044](https://doi.org/10.1016/j.rser.2017.10.044).
- [37] T. Xu et al., "A coordinated two-stage decentralized flexibility trading in distribution grids with MGs," *Prot. Control Mod. Power Syst.*, vol. 9, no. 5, pp. 54–69, Sep. 2024, doi: [10.23919/PCMP.2023.000178](https://doi.org/10.23919/PCMP.2023.000178).
- [38] "National solar radiation database." NREL. Accessed: Jul. 8, 2024. [Online]. Available: <https://nsrdb.nrel.gov/>
- [39] "Macao astronomical meteorological record station: Peizheng society of astronomy and meteorology." Accessed: Jul. 8, 2024. [Online]. Available: <https://std.pucniching.edu.mo/~pcmsams/index.php/weatherdata/weatherdata/>
- [40] "Australian apparent temperature (AT)." vCalc. Accessed: Feb. 8, 2025. [Online]. Available: <https://www.vcalc.com/wiki/australian-apparent-temperature>



**Taoyi Qi** (Graduate Student Member, IEEE) received the B.E. and M.E. degrees in electrical engineering from Zhejiang University, Hangzhou, China, in 2020 and 2023, respectively. He is currently pursuing the Ph.D. degree with the State Key Laboratory of Internet of Things for Smart City University of Macau, Macau, China, and the Laboratory of Internet of Things for Smart City, Advanced Research Institute in Hengqin, University of Macau, Zhuhai, China. His research interests mainly focus on demand response, intelligent buildings, and interactions between building energy consumption and climate diversity.



**Hongxun Hui** (Senior Member, IEEE) received the B.E. and Ph.D. degrees in electrical engineering from Zhejiang University, Hangzhou, China, in 2015 and 2020, respectively. From 2018 to 2019, he was a Visiting Scholar with the Advanced Research Institute, Virginia Tech, Blacksburg, VA, USA, and also with the CURENT Center, University of Tennessee, Knoxville, TN, USA. He is currently an Assistant Professor with the State Key Laboratory of Internet of Things for Smart City, University of Macau, Macau, China, and the Laboratory of Internet of Things for Smart City, Advanced Research Institute in Hengqin, University of Macau, Zhuhai, China. His research interests include optimization and control of power systems, demand response, and Internet of Things technologies for smart energy.



**Yonghua Song** (Fellow, IEEE) received the B.E. degree in electrical engineering from the Chengdu University of Science and Technology, Chengdu, China, in 1984, the Ph.D. degree in electrical engineering from China Electric Power Research Institute, Beijing, China, in 1989, the D.Sc. degree from Brunel University in 2002, the Honorary D.Eng. degree from the University of Bath in 2014, and the Honorary D.Sc. degree from the University of Edinburgh in 2019.

From 1989 to 1991, he was a Postdoctoral Fellow with Tsinghua University, Beijing, China. Then, he held various positions with Bristol University, Bristol, U.K.; Bath University, Bath, U.K.; and John Moores University, Liverpool, U.K., from 1991 to 1996. In 1997, he was a Professor of Power Systems with Brunel University, where he has been a Pro-Vice Chancellor for Graduate Studies since 2004. In 2007, he took up a Pro-Vice Chancellorship and Professorship of Electrical Engineering with the University of Liverpool, Liverpool. In 2009, he was with Tsinghua University as a Professor of Electrical Engineering and an Assistant President and the Deputy Director of the Laboratory of Low-Carbon Energy. From 2012 to 2017, he was the Executive Vice President of Zhejiang University, as well as the Founding Dean of the International Campus and a Professor of Electrical Engineering and Higher Education of the University. Since 2018, he has been a Rector with the University of Macau and the Director of the State Key Laboratory of Internet of Things for Smart City. Since 2019, he has been a Chairman with the Advanced Research Institute in Hengqin, University of Macau. His current research interests include smart grid, electricity economics, and operation and control of power systems.

Dr. Song was elected as the Vice-President of Chinese Society for Electrical Engineering (CSEE) and appointed as the Chairman of the International Affairs Committee of the CSEE in 2009. In 2004, he was elected as a Fellow of the Royal Academy of Engineering, U.K. In 2019, he was elected as a Foreign Member of the Academia Europaea.